Energy Transduction Optical Sensor in Skeletal Myosin†

Thomas P. Burghardt,*,‡ Sungjo Park,‡ Wen-Ji Dong,§ Jun Xing,§ Herbert C. Cheung,§ and Katalin Ajtai‡

Department of Biochemistry and Molecular Biology, Mayo Foundation, 200 First Street Southwest, Rochester, Minnesota 55905, and Department of Biochemistry and Molecular Genetics, University of Alabama at Birmingham, 1530 3rd Avenue South, MCLM 490, Birmingham, Alabama 35294-2041

Received May 23, 2002; Revised Manuscript Received January 29, 2003

ABSTRACT: The skeletal myosin cross-bridge in dynamic association with actin is the unitary energy transducer in muscle, converting free energy from ATP hydrolysis into contractile force. Myosin's conserved ATP-sensitive tryptophan (AST) is an energy transduction optical sensor signaling transduction-related transient conformation change by modulating its fluorescence intensity amplitude and relaxation rate. Recently introduced techniques have provided the means of observing the time-resolved intensity decay from this single residue in the native protein to elucidate the mechanism of its ATP sensitivity. AST signal characteristics could be derived from local protein structure by a scenario involving interactions with excited-state tryptophan. This investigation suggests the very different possibility that hypochromism induced in the tryptophan absorption band, a ground-state effect, is a significant structural effector of optical transduction sensing. This possibility makes feasible the interpretation of the transient AST optical signal in terms of dynamical protein structure, thereby raising the empirical signal to the level of a structural determinant. Using the crystallographically based geometry from several myosin structures, the maximum calculated AST hypochromism is <10% to be compared with the value of ∼30% observed here experimentally. Rationalizing the discrepancy invites further investigation of S1 dynamical structure local to the AST during transduction.

The myosin motor is the energy transducer in muscle, generating contractile force by converting free energy from ATP hydrolysis into work while interacting transiently with actin. ATP binding and hydrolysis occur in the myosin active site, initiating conformational change characterized as an open−closed transition within the head subfragment (subfragment 1 or S1) of the molecule (*2*). The open−closed transition involves a significant deformation of the converter domain peptide linking the semirigid catalytic and lever-arm domains making up S1. It is presumed that converter domain deformation with reversal of the open−closed transition occurs with the catalytic domain firmly bound to actin, causing lever-arm rotation and the linear translation of the S1 C-terminus relative to actin. Additional S1 C-terminus translation is also suggested to result from torque generated at the actomyosin interface with the transition from weak to strong actomyosin binding (*3*). The C-terminus translation against an opposing force produces work during contraction.

During the ATPase-powered open−closed structural transition, the switch II helix (amino acids 475−509)[1] changes position and internal structure (*2*, *4*), perturbing the local environment (*5*) of Trp510.[2] Perturbation of Trp510 affects its dipole moment and fluorescence intensity, giving rise to the ATP-sensitive tryptophan (AST) signal (*6*−*10*) that delineates the myosin ATPase intermediates (*11*, *12*). Previous observations of Trp510 fluorescence intensity amplitude and lifetime from rabbit skeletal myosin suggested tryptophan sensitivity to ATP hydrolysis involves the static quenching of Trp510 (*13*). Using crystal structures of skeletal (*14*), smooth muscle (*4*), and scallop (*15*) myosins, the computed overlap of electronic wave functions for Trp510 and vicinal residues identified interactions with Tyr503, Phe512, and Phe711 as potential quenchers. The groups responsible for the static quenching of Trp510 are collectively termed Q. The signature effect of the static quenching is the presence of delayed fluorescence in the AST signal. The contributions to the signal from delayed fluorescence increase with formation of the Trp510•Q complex, providing a longer fluorescence lifetime in the open conformation obtained without nucleotide. This work expands the Trp510 fluorescence decay data set, allowing quantitative evaluation of the full photophysical implications of the static quenching model. Our principal findings are 2-fold. First, static quenching upon formation of the Trp510•Q complex is due to hypochromism induced in the ^1L_a absorption band of Trp510. Second, the Trp510•Q excited-state complex (exiplex) emits fluorescence into the free tryptophan emission band with a quantum

† This work was supported by National Institutes of Health Grant R01 AR39288 and the Mayo Foundation.

* To whom correspondence should be addressed. Phone: (507) 284-8120. Fax: (507) 284-9349. E-mail: burghardt@mayo.edu.

‡ Mayo Foundation.

§ University of Alabama at Birmingham.

[1] The myosin sequence numbering is from chicken pectoralis muscle (*1*).

[2] Abbreviations: AST or Trp510, ATP-sensitive tryptophan; DcS1, *Dictyostelium* myosin subfragment 1; Q, vicinal Trp510 static quenching groups.

10.1021/bi026183e CCC: $25.00
Published on Web 04/25/2003

efficiency nearly equal to that of free Trp510.

Hypochromism is a ground-state effect routinely computed from structure (*16*), implying that quantitative changes in Trp510 fluorescence intensity can be readily calculated from the myosin crystal structures. Hypochromism, to the extent observed in skeletal myosin Trp510, is not fully represented in the skeletal (*14*), smooth (*4*), or scallop (*15*) S1 crystal structures for which we have already computed the Trp510 dipole moment (*13*). The latter suggests there may be a Trp510 hypochromism deficit for the interactions presently represented in the myosin crystal structures. It appears that we have not yet fully realized the structural manifestation of optical transduction sensing in myosin.

MATERIALS AND METHODS

Chemicals. ATP, ADP, dithiothreitol (DTT), TES, sodium azide, phenylmethanesulfonyl fluoride (PMSF), and Tris are from Sigma (St. Louis, MO). 5′-Iodoacetamidofluorescein (5′IAF) is from Molecular Probes (Eugene, OR). All other chemicals are reagent grade.

Solutions. A stock solution of $BeCl_2$ (88 mM Be, atomic absorption standard solution in 1% HCl) was adjusted to pH 5.0 by addition of NaOH. A potassium fluoride (KF) stock solution was prepared on the day it was used.

Preparation and Labeling of Myosin S1. Rabbit myosin was prepared from back and leg muscles by the method of Tonomura et al. (*17*). S1 was obtained by digestion of myosin filaments with α-chymotrypsin as described by Weeds and Taylor (*18*).

5′IAF modification of the highly reactive thiol (SH1 or Cys707) in S1 (F-S1) was carried out with a 1.8-fold molar excess of 5′IAF for 18−20 h at 4 °C in the dark as described previously (*19*). We incorporated 0.9 5′IAF group per S1 as inferred from K^+-EDTA and Ca^{2+}-ATPase activities (*20*, *21*). Unreacted 5′IAF was not removed from the F-S1 samples because its presence did not influence the tryptophan fluorescence observed in our experiments.

Myosin S1 ATPase. S1 ATPase activity was measured with the extent of inorganic phosphate production using the method of Fiske and Subbarow (*22*), and was expressed as a percent of control S1. K^+-EDTA ATPase measurements were taken on samples at 25 °C from 1 mL aliquots containing 0.26−0.35 μM S1, 2 mM ATP, 0.6 M KCl, 25 mM Tris-HCl (pH 8), and 6 mM EDTA. The level of Ca^{2+}-ATPase was measured as for K^+-EDTA ATPase except that 6 mM $CaCl_2$ replaced the 6 mM EDTA.

Preparation of Nucleotide-Bound or Trapped Nucleotide Analogue S1 and F-S1. Myosin S1 or F-S1 was trapped with beryllium or aluminum as described previously (*23*). When either S1 was trapped, K^+-EDTA activities for S1 and Ca^{2+} ATPase activities for F-S1 were inhibited by ≥90%. For fluorescence experiments in the presence of ADP (ATP), S1 or F-S1 was incubated with 1 mM $MgCl_2$ and 0.25 mM ADP (1 mM ATP).

Scheme 1

$$M+ATP \leftrightarrow M^*.ATP \leftrightarrow M^{**}.ADP.Pi \leftrightarrow M^{\wedge}.ADP + Pi \leftrightarrow M+ADP$$

Nucleotide Analogue Induced Structures of S1. The principal chemical states during S1 ATPase are collected in Scheme 1 where M, M*, M**, and M^ represent distinct myosin conformations. The steady-state fractional concentrations of the intermediates are known for a variety of myosins (*11*, *24*−*26*), all having the M**·ADP·P_i complex as the predominant intermediate (*27*).

Facilitating the structural characterization of the transients in Scheme 1 are nucleotide analogues. They reversibly trap the myosin active site and induce structures that statically mimic the transient intermediates in solution. Exhaustive comparison of analogue-induced and transient S1 structures led to the identification of bound ATPγS (*28*) or trapped ADP·BeF_x (low ionic strength) (*29*) with M*·ATP, trapped ADP·V_i, ADP·AlF_4^-, or ADP·BeF_x (high ionic strength) with M**·ADP·P_i, and bound ADP with M^·ADP (*30*−*33*). For reasons related to disruption and formation of a salt bridge adjacent to the active site, M, M*, and M^ are collectively termed "open" conformations while M** is termed a "closed" conformation (*2*).

Time-Resolved and Steady-State Fluorescence Measurements. Tryptophan fluorescence intensity decay was measured on two different time domain instruments.

At Mayo, fluorescence intensity relaxation was assessed on an analogue instrument with flash-lamp excitation (PTI, London, ON) described previously (*13*). Tryptophans were excited at 301 ± 5 nm, and emission was collected over a 16 nm bandwidth centered at 345 nm. Measurements on nucleotide analogue-trapped and ADP-bound protein were taken with 14 μM S1 in 1 mM DTT, 0.1 mM PMSF, and 25 mM TES (pH 7.0) at 7 °C. Measurements on ATP-bound protein had identical conditions except 3 μM S1 was used. All samples had an OD of <0.1 at 301 nm. Data collection intervals were 30−40 min on protein samples that had identical ATPases before and after the lifetime measurements.

At the University of Alabama at Birmingham, a laser-linked system was used. It consisted of a Mira 900-D dual picosecond and femtosecond mode-locked Ti:sapphire laser as the prime laser source, a Verdi 10 W solid-state Nd:vanadate laser as the pumping source for the prime laser, a Mira 900 D frequency doubler/tripler crystal assembly to generate the second and third harmonics for excitation, a Mira 9200 acoustic-optic pulse picker and a Bragg cell to reduce the pulse repetition rate to 4 MHz for photon counting, and a PicoQuant TimeHarp 200 photon counting system with 40 ps resolution. For the experiments presented here, vertically polarized 297 nm light generated from the prime laser was used for excitation. The emission was collected with a 340 nm three-cavity interference filter (10 nm half-width), and detected by a Hamamastu R3809U-50 microchannel plate PMT. Experimental conditions were identical to those used in the flash-lamp experiments except that the S1 concentration was 4 μM. Data collection intervals were ≤10 min for protein samples that had identical ATPases before and after the lifetime measurements. Collected data were analyzed as previously described (*34*).

Steady-state fluorescence intensity was measured on the PTI steady-state instrument. Tryptophans were excited at 301 ± 1 nm, and the emission spectrum was collected with 4 nm bandwidth resolution. Experimental conditions were identical to those used in the flash-lamp experiments except that the S1 or F-S1 concentration was 1 μM.

Time-resolved fluorescence intensities were fitted by convoluting the observed lamp profile with an exponential

fitting function of the form

$$F(t) = \sum_{i=1}^{p} A_i e^{-t/\tau_i} \quad (1)$$

where A_i is the decay amplitude and τ_i the lifetime for the *i*th component (*35*). Best fits for curves generated by the flash-lamp system were located using a global nonlinear least-squares protocol applied to multiple, independently measured, fluorescence intensity relaxation curves. Intensity decay curves generated by the laser-based system were fitted individually. Trp510 fluorescence decay curves from both the flash-lamp and laser-based systems were monoexponential and fully characterized by one term in the sum of eq 1. We verified the flash-lamp instrument calibration using NATA in 0.1 M sodium phosphate (pH 7) at 20 °C having a lifetime of 3 ns and quinine bisulfate in 0.1 N H_2SO_4 at 23 °C having a lifetime of 18.9 ns. These standards gave 2.95 ± 0.3 and 19.4 ± 0.2 ns, respectively. We verified the ability of the flash-lamp instrument to resolve multiple tryptophan fluorescence lifetimes by analyzing the total tryptophan fluorescence intensity decay of S1. From the S1, we obtained three lifetimes of 0.5 ± 0.2, 3.7 ± 0.1, and 8.6 ± 0.4 ns, in good agreement with previous measurements (*10*).

Under some circumstances, sample rotational diffusion can influence the observed fluorescence lifetime. We removed sample rotational relaxation effects from emission intensity relaxation in the flash-lamp system by exciting with naturally polarized light and collecting emitted light through an emission polarizer oriented 35.3° from the vertical (*35*). In the laser-based system, we used magic angle conditions (excitation vertically polarized and emission polarized at the magic angle of 54.7° from the vertical) (*35*). We observed no systematic difference in the observed lifetime of Trp510 with and without the polarizers, suggesting rotational relaxation makes no contribution. Results shown below originate from measurements without polarizers.

Isolation of Trp510 Fluorescence Emission. Chymotryptic rabbit skeletal S1 contains five tryptophan residues at positions 113, 131, 440, 510, and 595. Difference spectroscopy between S1 samples containing perturbed and unperturbed Trp510 isolates Trp510 emission from the total tryptophan fluorescence signal. Trp510 spectroscopic perturbants include fluorescein covalently linked to SH1 in S1 and shown previously to selectively quench Trp510 fluorescence (*5*, *36*). While Trp131 detects nucleotide binding by a slight intensity enhancement, fluorescein at SH1 eliminates AST intensity enhancement upon nucleotide binding to the S1 active site, indicating that for practical purposes Trp510 is the sole AST in skeletal S1 (*37*). Consistent with the latter finding, in skeletal S1, selective tryptophan photochemical modification by 2,2,2-trichloroethanol (TCE) showed the AST to be a single solvent-exposed residue likely to be Trp510 (*38*), while spectroscopic deconvolution of total tryptophan emission identified Trp510 as an AST (*39*). In other S1 isoforms, single tryptophan mutants of smooth muscle S1 containing Trp440, -510, or -595 confirmed AST identification with Trp510 (*40*−*42*), while complementary results were also obtained from a single tryptophan mutant of *Dictyostelium* S1 (DcS1) (*43*). The apparent equivalence of the AST and Trp510 implies that the nucleotide bound to the S1 active site likewise selectively perturbs Trp510 emission.

Scheme 2

$$\begin{array}{lcl} W_{510}{}^* + Q & \underset{k_{W^*\leftarrow E^*}}{\overset{k_{E^*\leftarrow W^*}}{\rightleftharpoons}} & (W_{510}\cdot Q)^* \\ R_W \Downarrow k_{W^*} & & k_{E^*} \Downarrow R_E \\ W_{510} + Q & \rightleftharpoons & (W_{510}\cdot Q) \end{array}$$

In the work presented here, we utilize two differential spectroscopic methods for Trp510 emission isolation. Method 1 involves the fluorescein group and signal ΔI_1 defined by

$$\Delta I_1(N,t) \equiv I(S1{\cdot}N,t) - I(F\text{-}S1{\cdot}N,t) \quad (2)$$

where t is time, I is the tryptophan fluorescence intensity, and N represents a nucleotide bound to the active site or, when absent, the no nucleotide form. Method 2 involves the bound nucleotide, N, and signal ΔI_2 defined by

$$\Delta I_2(N,t) \equiv I(S1{\cdot}N,t) - I(S1,t) \quad (3)$$

Method 1 isolates a homogeneous Trp510 emission originating from S1 in a single conformation. Method 2 isolates a heterogeneous Trp510 emission originating from S1 in the presence and absence of nucleotide (*37*).

Modeling and Data Analysis. Time-resolved fluorescence intensity decay isolated by method 1 or 2 provides amplitude and relaxation characteristics modeled by the mechanism in Scheme 2 involving Trp510 (W) and a static quencher (Q) when free or in complex (E), in a ground or excited (*) state (*44*).

The rates defined in Scheme 2 include the free Trp510 absorption rate, R_W, the free Trp510 fluorescence intensity decay rate in the absence of Q, k_{W^*}, the dynamic quenching rate proportional to the concentration of Q, $k_{E^*\leftarrow W^*}[Q]$, the complexed Trp510 dissociation rate, $k_{W^*\leftarrow E^*}$, the complexed Trp510 absorption rate, R_E, and the complexed Trp510 fluorescence intensity decay rate in the absence of dissociation, k_{E^*}. Other useful parameters are the ratio of extinction coefficients for free and complexed Trp510 ($\beta = \epsilon_E/\epsilon_W = k_{FE}/k_{FW}$, where k_{FW} and k_{FE} are the natural fluorescence relaxation rates) and the fractional concentration of the ground-state complex [$\alpha = [E]/([E] + [W]) = [E]/[W]_0$, where $[W]_0$ is the total local concentration of Trp510]. Then the dynamic quenching rate is re-expressed as $k_{E^*\leftarrow W^*}[W]_0(1 - \alpha) = k^0{}_{E^*\leftarrow W^*}(1 - \alpha)$ because $[Q] = [W]$ and $1 - \alpha = [W]/[W]_0$, and we combined the product of the two unknown constants $k_{E^*\leftarrow W^*}[W]_0$ into $k^0{}_{E^*\leftarrow W^*}$. The emitted Trp510 intensity is the sum of intensities from the free and complexed species. Previously, we neglected the contribution from the complexed species (*13*). The method 1 time-resolved fluorescence relaxation curve, $\Delta I_1(N,t)$, appropriate for the Scheme 2 model is obtained from the ordinary differential equations described previously (see eq 5 in ref *13*), giving

$$\Delta I_1(N,t) = C_0 e^{1/2(\Omega+\lambda)t}\left(\left\{\frac{1-\alpha}{2}\left[1 + e^{-\lambda t} + \frac{\Delta}{\lambda}(1 - e^{-\lambda t})\right] + \beta\alpha(1 - e^{-\lambda t})\frac{k_{W^*\leftarrow E^*}}{\lambda}\right\}\rho_W + \beta\left\{\frac{\alpha}{2}\left[1 + e^{-\lambda t} - \frac{\Delta}{\lambda}(1 - e^{-\lambda t})\right] + \beta(1-\alpha)^2(1 - e^{-\lambda t})\frac{k^0{}_{E^*\leftarrow W^*}}{\lambda}\right\}\rho_E\right) \quad (4)$$

where $\Omega = -k_{W^*} - k^0_{E^*\leftarrow W^*}(1-\alpha) - k_{W^*\leftarrow E^*} - k_{E^*}$, $\Delta = \Omega + 2(k_{W^*\leftarrow E^*} + k_{E^*})$, and $\lambda = [4k_{W^*\leftarrow E^*}k^0_{E^*\leftarrow W^*}(1-\alpha) + \Delta^2]^{1/2}$. C_0 is a constant set by an arbitrary intensity normalization; ρ is the normalized emission line shape, and α is the only parameter (implicitly) dependent on N. The method 2 time-resolved fluorescence relaxation curve, $\Delta I_2(N,t)$, is obtained from eq 4 and

$$\Delta I_2(N,t) = \Delta I_1(N,t) - \Delta I_1(-,t) \quad (5)$$

The Trp510 relative quantum efficiency, the ratio of time-integrated fluorescence intensities in the presence (ϕ) and absence (ϕ_0) of Q, is from eq 4

$$\frac{\phi}{\phi_0} = \frac{\phi_W}{\phi_0} + \frac{\phi_E}{\phi_0} = \frac{1-\alpha[1-(1-p)\beta]}{1+\frac{k^0_{E^*\leftarrow W^*}}{k_{W^*}}p(1-\alpha)} + \frac{p\beta\gamma\left[(1-\alpha)(1-\alpha+\alpha\beta)\frac{k^0_{E^*\leftarrow W^*}}{k_{E^*}} + \alpha\beta\frac{k_{W^*}}{k_{E^*}}\right]}{1+\frac{k^0_{E^*\leftarrow W^*}}{k_{W^*}}p(1-\alpha)} \quad (6)$$

where $p = k_{E^*}/(k_{E^*} + k_{W^*\leftarrow E^*})$ and γ ($\equiv \rho_E/\rho_W$) is the detected relative emission intensity due to line shape.

Time-resolved intensities $\Delta I_1(N,t)$ and $\Delta I_2(N,t)$ were observed for the S1 transient intermediate conformations in Scheme 1. These intensities were also expressed in terms of the model parameters α, β, and the rates appearing in Scheme 2 by using eqs 4 and 5 and the normalization constant C_0, which equals $1/[1 + \alpha_0(\beta\gamma - 1)]$ for $\Delta I_1(-,t=0) \equiv 1$, and the fractional concentration of the complex in the absence of nucleotide (α_0). Observed time-zero amplitudes for ΔI_1 and ΔI_2, corresponding to each S1 conformation that was investigated, were fitted simultaneously with the model-derived expressions determining a set of equally good choices for $\beta\gamma$ and the α values by a constrained linear least-squares protocol. Members in this set were substituted into the model-derived expressions for ΔI_1 and ΔI_2. Observed $\Delta I_1(N,t)$ and $\Delta I_2(N,t)$ time-dependent curves, corresponding to each S1 conformation that was investigated, were fitted simultaneously with the model-derived expressions by a nonlinear least-squares protocol determining the best choices for β and the rates appearing in Scheme 2 (except for R_W and R_E) for the given $\beta\gamma$ and the α values. A global best fit matching $\beta\gamma$, α values, β, and rates determined all parameters in the model system and the quantum efficiencies in eq 6.

Published time-resolved fluorescence intensity decay data from the AST in DcS1 were used to determine the Scheme 2 parameters in this system (*45*). The data have the form of ΔI_1 and were analyzed using the protocol described above.

RESULTS

Method 2 Trp510 Time-Resolved Fluorescence Intensity Decay. Figure 1 shows $\Delta I_2(N,t)$ from eq 3 for S1·ADP·AlF_4^- (●) and S1·ADP·BeF_x (○). The top panel of Figure 1 shows typical decay curves observed using the flash-lamp system, while the bottom panel shows the equivalent curves obtained using the laser-based system. A single-exponential fitting function in the form of eq 1 provides the amplitude (A) and lifetime (τ) for the Trp510 fluorescence decay. Residuals and their autocorrelation, shown only for the less intense curves, indicate that the data are approximated well by the single-exponential function. $\Delta I_2(N,t)$ was also obtained for S1·ADP and S1·ATP using the flash-lamp system (data not shown).

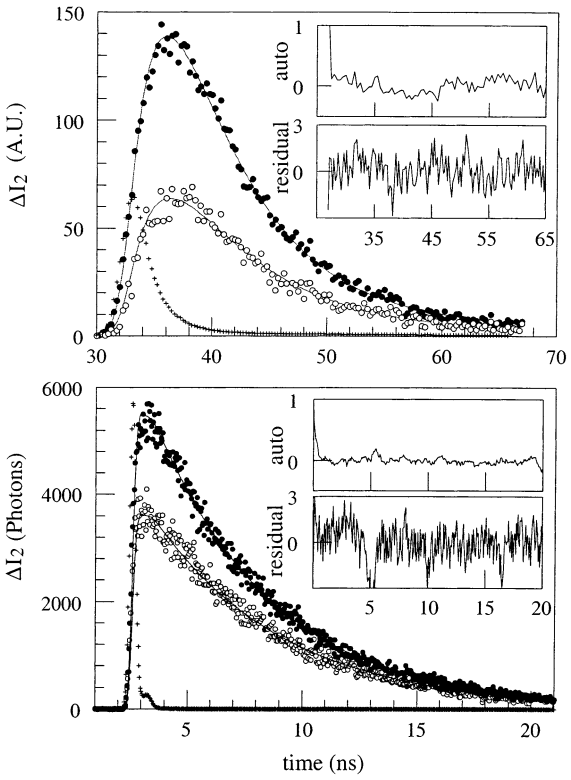

FIGURE 1: Method 2 isolation of Trp510 time-resolved fluorescence intensity (ΔI_2) from S1·ADP·BeF_x (○) and S1·ADP·AlF_4^- (●) following flash-lamp (top) or laser (bottom) excitation. A.U. is for arbitrary units in the top panel. The lamp intensities are normalized to have a common scale with the fluorescence data. The solid lines are best theoretical fits for a single-exponential fitting function from eq 1. The residuals that are depicted are the difference between the data and the best fitting theoretical curve for the S1·ADP·BeF_x sample. Similar residuals were obtained for the S1·ADP·AlF_4^- sample. Autocorrelation of the residuals (auto), amplifying systematic deviations between data and fit, shows deviations are random (except for the rf noise in the case of the flash lamp).

$\Delta I_2(N,t)$ decays as a sum of four exponentials in Scheme 2 as indicated by eqs 4 and 5. Nonetheless, the characterization of the relaxation curve as monoexponential does not in itself imply a discrepancy with Scheme 2 or a fundamental property of Trp510 but instead expresses the resolution with which we can observe intensity relaxation. We demonstrated this using the Trp510 intensity relaxation parameters described below to back-calculate the expected sum of four exponential relaxations for the M, M^, M*, and M** conformations. To these simulated curves we added random noise with amplitude to approximate that in the experimental data, and we then fitted them as we did the real experimental data. The simulated data are monoexponential to the extent that the use of two or more exponential relaxation functions did not improve the goodness of the fit. We did not simulate lamp deconvolution since this exercise could only weaken our ability to resolve multiple relaxations.

Table 1 summarizes Trp510 fluorescence intensity amplitudes and lifetimes isolated by either method 1 or 2. The amplitudes and lifetimes derived from method 1 are from

Table 1: Time-Resolved Trp510 Fluorescence in Skeletal S1[a]

nucleotide or analogue (N)	conformation (Scheme 1)	method 1[b] lifetime τ (ns)	method 1[b] amplitude A (AU)	method 2 lifetime	method 2 amplitude
–	M	9.4 ± 0.2	1.00 ± 0.03 (5)	-	-
ADP	M^	9.2 ± 0.2	1.06 ± 0.03 (4)	8.4 ± 0.6	0.11 ± 0.005 (12)
ADP·BeF_x	M*	8.0 ± 0.2	1.72 ± 0.19 (2)	5.6 ± 0.1	0.54 ± 0.04 (9)[c]
ADP·AlF_4^-	M**	7.0 ± 0.3	2.14 ± 0.25 (3)	4.8 ± 0.1	1.26 ± 0.05 (9)[c]
ATP		7.2 ± 0.3	2.00 ± 0.17 (4)	5.0 ± 0.2	1.24 ± 0.11 (6)

[a] The mean standard errors for n independent measurements are indicated. Lifetimes and amplitudes are defined in eq 1, and both are determined in a single measurement. All amplitudes share a common scale expressed in the arbitrary units (AU) with $\langle \Delta I_1(-,t=0) \rangle \equiv 1$. [b] Method 1 data taken from ref *13*. [c] The fluorescence intensity decays measured by the laser-based instrument contributed single method 2 Trp510 relaxation curves for the S1 conformations induced by ADP·BeF_x and ADP·AlF_4^-. Fitted independently, these curves had amplitudes of 0.7 and 1.1, and, lifetimes of 5.6 and 5.1 ns for the ADP·BeF_x and ADP·AlF_4^- analogues, respectively. These amplitudes and lifetimes are within the standard error of the quantities observed with the flash-lamp instrument. Values quoted in the table are an average over all measurements.

Table 2: Rate Parameters and β for the Optical Transduction Sensor in Skeletal and *Dictyostelium* S1[a]

parameter	skeletal S1	DcS1[b]
k_{W^*} (ns^{-1})	0.129 ± 0.001	0.238 ± 0.006
$k^0_{E^*\leftarrow W^*}$ (ns^{-1})	0.039 ± 0.002	0.010 ± 0.01
$k_{W^*\leftarrow E^*}$ (ns^{-1})	0.059 ± 0.002	0.14 ± 0.03
k_{E^*} (ns^{-1})	0.122 ± 0.005	1.50 ± 0.08
β	0.70 ± 0.05	0.80 ± 0.1

[a] Errors indicate standard deviation estimates based on the goodness of the fit of the time-resolved fluorescence intensity relaxations. Rate parameters are defined in Scheme 2. $\beta = \epsilon_E/\epsilon_W$, the ratio of extinction coefficients for complexed and free Trp510. [b] Values computed with data taken from ref *45*.

Table 3: Relative Quantum Efficiencies and α Values for the Optical Transduction Sensor in Skeletal and *Dictyostelium* S1[a]

nucleotide or analogue (N)	conformation (Scheme 1)	α skeletal	α Dc	ϕ_W/ϕ_0[b] skeletal	ϕ_W/ϕ_0[b] Dc	ϕ_E/ϕ_0[b] skeletal	ϕ_E/ϕ_0[b] Dc
-	M	0.9−1.0	0.5	0.24	0.55	0.20	0.03
ADP	M^	0.8−1.0	0.7	0.30	0.39	0.18	0.04
ADP·BeF_x	M*	0.5−0.7	–	0.50	–	0.14	–
ADP·AlF_4^-	M**	0.0−0.2	0	0.76	0.96	0.08	0.00
ATP		0.1−0.3	0	0.75	0.96	0.09	0.00

[a] The range of values indicates standard deviation estimates based on the goodness of the fit of the time-resolved fluorescence intensity relaxation. α, the fractional concentration of complexed Trp510, and ϕ_W/ϕ_0 and ϕ_E/ϕ_0, the relative quantum efficiencies of the free and complexed form of Trp510, respectively, depend on the active site substrate occupant (N) or equivalently the S1 conformation from Scheme 1. Quantum efficiencies depend on γ (eq 6) for which we found $\gamma = 0.60$ and 0.65 with skeletal and DcS1, respectively. [b] Values for DcS1 computed with data taken from (ref *45*. No error estimates are available for the DcS1 data.

previously published data (*13*). Amplitudes and lifetimes derived from method 2 are computed from the data in Figure 1 averaged with amplitudes and lifetimes computed from seven parallel experiments. Amplitudes and lifetimes were similarly computed for S1·ADP and S1·ATP. As observed previously, the Trp510 intensity relaxation time decreases when S1 assumes more closed conformations with a bound or trapped nucleotide or nucleotide analogue.

Table 2 compares β and the rate parameters characterizing AST emission for S1 and DcS1. Parameter β and the rates are intrinsic properties of Trp510 fluorescence that are intimately related to the ground- and excited-state coordination of the Trp510·Q complex, respectively, in the Scheme 2 model. When skeletal S1 is considered, the four rates governing fluorescence relaxation have similar amplitudes, implying each process contributes appreciably to the intensity decay. Exiplex dissociation ($k_{W^*\leftarrow E^*}$) permits the Trp510·Q complex to act as an excited-state reservoir that replenishes W* after time zero, giving rise to delayed fluorescence and the unusually long apparent tryptophan lifetime observed in the open conformation. The dynamic quenching rate, $k^0_{E^*\leftarrow W^*}(1 - \alpha)$, reduces the intensity relaxation time as S1 assumes the more closed conformations where complex formation is less likely. Exiplex relaxation by decay to the ground state is like that of free Trp510 relaxation, implying that the expected rapid decay of the exiplex does not occur. Q interacts with Trp510 by forming both ground- and excited-state complexes. The ground-state complex diminishes light absorption in the tryptophan ^1L_a band, an observation quantified by parameter β being <1, lowering the fluorescence intensity amplitude in the open S1 conformation (Table 1). The exiplex diminishes light emission by providing an alternative channel for excited-state relaxation without photon emission. In DcS1, rates are larger except for the negligible dynamic quenching rate, $k^0_{E^*\leftarrow W^*}$. The exiplex relaxation rate in the absence of dissociation, k_{E^*}, is 1 order of magnitude larger than in skeletal S1 and is the most rapid process in the system, essentially eliminating any noticeable contribution from delayed fluorescence or exiplex emission. In DcS1, parameter β continues to be significantly <1.

Table 3 compares α values for S1 and DcS1. The α values depend on the S1 conformation induced by the ligand in the active site and characterize protein conformation local to, but not the optical properties of, the emitting group. In skeletal S1, the observed α values show that the no nucleotide and the ADP·AlF_4^--induced conformations occupy the extreme associated and dissociated states, respectively, in Scheme 2 while ADP and ADP·BeF_x-induced conformations are intermediate. This is as expected from earlier work showing that AST fluorescence was not affected by ionic perturbants of S1 structure when S1 assumed no nucleotide and ADP·AlF_4^--induced conformations while increasing ionic strength drove the aforementioned intermediate conformations toward full dissociation (*29*). It appears that the Trp510·Q complex in the no nucleotide conformation is too stable to be perturbed by ionic strength. DcS1 is in qualitative agreement with the skeletal S1 results, although the no nucleotide and ADP-induced conformations reverse roles.

The observed quantum efficiencies in Table 3 depend on both the intrinsic properties of Trp510 fluorescence and on the S1 conformation induced by the active site ligand. Considering first skeletal S1, we find that in the no nucleotide

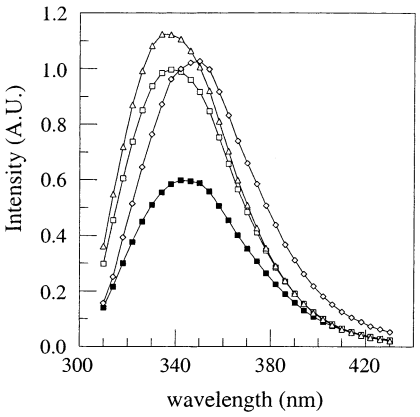

FIGURE 2: Method 1 isolation of steady-state Trp510 fluorescence emission for S1 (■) and S1·ADP·AlF_4^- (□). Pure exiplex (◇) and uncomplexed (△) Trp510 emission line shapes were computed from the total Trp510 emission in the presence and absence of nucleotide or nucleotide analogue using eq 7 as described in the Results.

and ADP-induced S1 conformations the exiplex contributes nearly one-half of the total emitted intensity. Exiplex emission declines as S1 assumes the closed conformation. In DcS1, the no nucleotide and ADP-induced conformations have exiplex contributions of <10% of the total emitted intensity. The exiplex contributes negligibly when DcS1 assumes the closed conformation.

Method 1 Trp510 Steady-State Fluorescence Emission Spectra. Figure 2 shows the Trp510 steady-state emission spectrum for S1 (■) and S1·ADP·AlF_4^- (□) isolated by method 1. Trp510 steady-state emission spectra were likewise observed for S1·ADP and S1·ADP·BeF_x (data not shown). The emission spectra show no indication of a distinct exiplex contribution, suggesting it emits into the broad envelope of the tryptophan ^1L_a emission band. We separated contributions from free and complexed Trp510 using the data in Figure 2 and those from the S1·ADP and S1·ADP·BeF_x species.

Substituting constants from Tables 2 and 3 into eqs 2 and 4, and then integrating over time to convert time-resolved to steady-state quantities, we obtain the following constraints on the steady-state intensities:

$$\begin{aligned}\Delta I_{1,ss}(-) &= 0.24\rho_W + 0.35\rho_E\\ \Delta I_{1,ss}(\mathrm{ADP}) &= 0.30\rho_W + 0.32\rho_E\\ \Delta I_{1,ss}(\mathrm{BeF}_x) &= 0.50\rho_W + 0.24\rho_E\\ \Delta I_{1,ss}(\mathrm{AlF_4^-}) &= 0.76\rho_W + 0.15\rho_E\end{aligned} \quad (7)$$

Solving for ρ_W and ρ_E using linear least-squares, we obtain the line shapes for the free (△) and complexed (◇) forms of Trp510 shown in Figure 2. We see exiplex emission is red shifted compared to that from free Trp510.

DISCUSSION

Modulation of an optical signal directly attributable to the highly conserved Trp510 residue in skeletal (*37*, *38*, *46*), smooth muscle (*41*, *42*), and *Dictyostelium* (*43*, *45*, *47*) S1 accompanies myosin ATPase. The signal is manifested as an increase in the Trp510 dipole moment (*6*) and steady-state fluorescence intensity (*8*) as the S1 transits from open to closed conformations. Time-resolved Trp510 fluorescence intensity decay in skeletal myosin has indicated a static quenching mechanism causes intensity and lifetime modulation (*13*). Comparison of S1 crystal structures representing open and closed conformations suggests the effect results from rigid rotation and slight deformation of the switch II helix (*2*, *4*). These structural changes, driven by ATP hydrolysis, cause rearrangement of Trp510 relative to Tyr503, Phe515, Phe711, and other spectroscopically active groups in the vicinity that perturb the electronic wave function of Trp510 and modulate its absorption and fluorescence signal (*13*). Qualitatively similar conclusions have been formed from Trp510 time-resolved fluorescence in DcS1 (*45*).

The applicability of Scheme 2 to the Trp510 absorption and fluorescence modulation mechanism was qualitatively established previously by observing a steadily increasing fluorescence lifetime in S1 as it assumes more open conformations (*13*). This effect results from the larger delayed fluorescence contribution to the total Trp510 fluorescence signal as the equilibrium between free and complexed Trp510 shifts toward the complexed form. Emission from the exiplex contributes fluorescence by first dissociating, E* → W* + Q, and then emitting from the W* state. The two-step process delays the initiation of photon emission, and thus delays fluorescence. By the addition of data from the method 2 isolation of Trp510 fluorescence described here, we have sufficient constraints to make reliable estimates for the adjustable parameters of the Scheme 2 model.

We now find that the exiplex relaxation rate, k_{E*}, is approximately equal to the free Trp510 relaxation rate, k_{W*}, and that the extinction coefficient ratio $\beta < 1$. This unexpectedly small k_{E*} provides an exiplex that is sufficiently stable to contribute to Trp510 fluorescence either by dissociation to W* and then emission or by direct photon emission. The former was evidently anticipated, but the latter is more novel exiplex behavior. β measures hypochromism induced in the ^1L_a absorption band of the Trp510 indole by ground-state complex formation with Q. The hypochromism is responsible for the Trp510 fluorescence intensity amplitude modulation accompanying nucleotide binding to S1. This finding explains why the AST in skeletal myosin was first observed using absorption (*6*). Methods for computing optical signals originating from ground-state Trp510 (like circular dichroism and absorption) are routine and accurate given the structure (*16*, *48*). They are also used successfully in the converse problem where structure is surmised from the optical signal (*49*). Excited-state signals (like fluorescence) are much more difficult to interpret structurally. Our results imply that computation of the hypochromism in the ^1L_a band of Trp510, a computation we already perform on S1 crystal structures, will emulate the optical transduction sensor. The similar analysis of time-resolved fluorescence intensity decay data from DcS1 (*45*) suggests that, although the geometry of the Trp510·Q exiplex differs from that in skeletal S1, the underlying cause of the AST signal modulation is the same.

An alternative to the Scheme 2 model has Trp510 interacting with various groups in its vicinity with the predominant interaction differing for each Scheme 1 intermediate. Then exiplex photophysics would figure more prominently in the characterization of the optical transduction sensor. In particular, each transient S1 conformation would produce a new set of exiplex characteristic rates k_{E*}, $k_{W*\leftarrow E*}$,

and $k^0_{E^*\leftarrow W^*}$. Arguing against this possibility are observations from the AST in DcS1 (*45*). There, two nearly constant fluorescence lifetimes of 1 and 5 ns characterized every transient intermediate of DcS1 that was investigated. The shorter lifetime is derived principally from exiplex relaxation, demonstrating a constant set of rate parameters characterize its photophysical properties in accordance with Scheme 2. This clear delineation of emitting species did not occur with skeletal S1 because the W* and E* species have indistinguishable relaxation times.

The observed β (Table 2) is smaller than expectations from computation based on skeletal (*14*), smooth (*4*), or scallop (*15*) S1 crystal structures for which we obtain a β between 0.94 and 1 (see Table 2 in ref *13* where $1/\beta$ is computed). Apparently, the native system in solution more effectively couples Trp510 and quencher electronic wave functions. The average Trp510·Q structure determined by crystallography may not accurately represent the ensemble average structure that would produce the observed optical signature. This could come about, for instance, if the optical signal weights structures in an ensemble representing S1 in a manner different from the electron density observed in X-ray diffraction. We will need to find the "missing" Trp510 hypochromism by fashioning a new proposal for the Trp510−Q interaction in skeletal S1 during transduction within the context of the transduction model recently introduced (*50*).

CONCLUSION

Quantitative estimates of Scheme 2 parameters representing the mechanism for modulating absorption and fluorescence from the AST indicate hypochromism in the ^1L_a absorption band of Trp510 is the cause of static quenching when S1 assumes an open conformation. Hypochromism is a ground-state effect that can be readily calculated by standard methods, suggesting the optical transduction sensor signal is structurally interpretable. The induced hypochromism was traced to the ground-state interaction of Trp510 with one or more residues, including Tyr503, Phe512, Phe711, or other spectroscopically active groups in the vicinity. This complex forms an exiplex that emits with both prompt and delayed fluorescence. Using the crystallographically based geometry from several myosin structures, calculation of the hypochromism in the AST indicates a signal deficit compared to that observed experimentally, recommending, and giving direction to, the search for a new dynamical model for structure local to the AST during transduction.

ACKNOWLEDGMENT

We thank Susanna P. Garamszegi for technical assistance and Dr. Mihály Kovács from the National Institutes of Health for helpful discussions.

REFERENCES

1. Maita, T., Yajima, E., Nagata, S., Miyanishi, T., Nakayama, S., and Matsuda, G. (1991) *J. Biochem. 110*, 75−87.
2. Geeves, M. A., and Holmes, K. C. (1999) *Annu. Rev. Biochem. 68*, 687−728.
3. Root, D. D., Stewart, S., and Xu, J. (2002) *Biochemistry 41*, 1786−1794.
4. Dominguez, R., Freyzon, Y., Trybus, K. M., and Cohen, C. (1998) *Cell 94*, 559−571.
5. Park, S., Ajtai, K., and Burghardt, T. P. (1996) *Biochim. Biophys. Acta 1296*, 1−4.
6. Morita, F. (1967) *J. Biol. Chem. 242*, 4501−4506.
7. Cheung, H. C., and Morales, M. F. (1969) *Biochemistry 8*, 2177−2182.
8. Werber, M. M., Szent-Györgyi, A. G., and Fasman, G. D. (1972) *Biochemistry 11*, 2872−2883.
9. Bivin, D. B., Kubota, S., Pearlstein, R., and Morales, M. F. (1993) *Proc. Natl. Acad. Sci. U.S.A. 90*, 6791−6795.
10. Torgerson, P. M. (1984) *Biochemistry 23*, 3002−3007.
11. Trentham, D. R., Eccleston, J. F., and Bagshaw, C. R. (1976) *Q. Rev. Biophys. 9*, 217−281.
12. Johnson, K. A., and Taylor, E. W. (1978) *Biochemistry 17*, 3432−3442.
13. Park, S., and Burghardt, T. P. (2002) *Biochemistry 41*, 1436−1444.
14. Rayment, I., Rypniewski, W. R., Schmidt-Base, K., Smith, R., Tomchick, D. R., Benning, M. M., Winkelmann, D. A., Wesenberg, G., and Holden, H. M. (1993) *Science 261*, 50−58.
15. Houdusse, A., Kalabokis, V. N., Himmel, D., Szent-Gyorgyi, A. G., and Cohen, C. (1999) *Cell 97*, 459−470.
16. Bayley, P. M., Nielsen, E. B., and Schellman, J. A. (1969) *J. Phys. Chem. 73*, 228−243.
17. Tonomura, Y., Appel, P., and Morales, M. (1966) *Biochemistry 5*, 515−521.
18. Weeds, A. G., and Taylor, R. S. (1975) *Nature 257*, 54−56.
19. Ajtai, K., and Burghardt, T. P. (1992) *Biochemistry 31*, 4275−4288.
20. Ajtai, K., Poto, L., and Burghardt, T. P. (1990) *Biochemistry 29*, 7733−7741.
21. Ajtai, K., Ilich, P. J. K., Ringler, A., Sedarous, S. S., Toft, D. J., and Burghardt, T. P. (1992) *Biochemistry 31*, 12431−12440.
22. Fiske, C. H., and Subbarow, Y. (1925) *J. Biol. Chem. 66*, 375−400.
23. Park, S., Ajtai, K., and Burghardt, T. P. (1999) *Biochim. Biophys. Acta 1430*, 127−140.
24. Marston, S. B., and Taylor, E. W. (1980) *J. Mol. Biol. 139*, 573−600.
25. Taylor, R. S., and Weeds, A. G. (1976) *Biochem. J. 159*, 301−315.
26. Murhpy, C. T., Rock, R. S., and Spudich, J. A. (2001) *Nat. Cell Biol. 3*, 311−315.
27. Bagshaw, C. R., and Trentham, D. R. (1974) *Biochem. J. 141*, 331−349.
28. Goody, R. S., and Hofmann, W. (1980) *J. Muscle Res. Cell Motil. 1*, 101−115.
29. Peyser, Y. M., Ajtai, K., Burghardt, T. P., and Muhlrad, A. (2001) *Biophys. J. 81*, 1101−1114.
30. Fisher, A. J., Smith, C. A., Thoden, J. B., Smith, R., Sutoh, K., Holden, H. M., and Rayment, I. (1995) *Biochemistry 34*, 8960−8972.
31. Werber, M. M., Peyser, Y. M., and Muhlrad, A. (1992) *Biochemistry 31*, 7190−7197.
32. Peyser, Y. M., Ajtai, K., Werber, M. M., Burghardt, T. P., and Muhlrad, A. (1997) *Biochemistry 36*, 5170−5178.
33. Maruta, S., Henry, G. D., Sykes, B. D., and Ikebe, M. (1993) *J. Biol. Chem. 268*, 7093−7100.
34. Dong, W.-J., Chandra, M., Xing, H., Solaro, R. J., and Cheung, H. C. (1997) *Biochemistry 36*, 6745−6753.
35. Badea, M. G., and Brand, L. (1979) *Methods Enzymol. 61*, 378−425.
36. Park, S., Ajtai, K., and Burghardt, T. P. (1996) *Biophys. Chem. 63*, 67−80.
37. Park, S., and Burghardt, T. P. (2000) *Biochemistry 39*, 11732−11741.
38. Papp, S., and Highsmith, S. (1993) *Biochim. Biophys. Acta 1202*, 169−172.
39. Reshetnyak, Y., Andreev, O., Borejdo, J., Toptygin, D., Brand, L., and Burstein, E. A. (2000) *J. Biomol. Struct. Funct. 18*, 113−125.
40. Sperber, M. F., van Duffelen, M., Chrin, L. R., and Berger, C. L. (2002) *Biophys. J. 82*, 367a.
41. Yengo, C. M., Chrin, L. R., Rovner, A. S., and Berger, C. L. (2000) *J. Biol. Chem. 275*, 25481−25487.

42. Onishi, H., Konishi, K., Fujiwara, K., Hayakawa, K., Tanokura, M., Martinez, H. M., and Morales, M. F. (2000) *Proc. Natl. Acad. Sci. U.S.A. 97*, 11203−11208.
43. Batra, R., and Manstein, D. J. (1999) *J. Biol. Chem. 380*, 1017−1023.
44. Birks, J. B. (1970) in *Photophysics of Aromatic Molecules*, pp 403−491, Wiley-Interscience, London.
45. Malnasi-Csizmadia, A., Kovacs, M., Woolley, R. J., Botchway, S. W., and Bagshaw, C. R. (2001) *J. Biol. Chem. 276*, 19483−19490.
46. Hiratsuka, T. (1992) *J. Biol. Chem. 267*, 14949−14954.
47. Malnasi-Csizmadia, A., Pearson, D. S., Kovacs, M., Woolley, R. J., Geeves, M. A., and Bagshaw, C. R. (2001) *Biochemistry 40*, 12727−12737.
48. Ajtai, K., Peyser, Y. M., Park, S., Burghardt, T. P., and Muhlrad, A. (1999) *Biochemistry 38*, 6428−6440.
49. Burghardt, T. P., Juranic, N., Macura, S., Muhlrad, A., and Ajtai, K. (1999) *J. Am. Chem. Soc. 121*, 10373−10378.
50. Muhlrad, A., Peyser, Y. M., Nili, M., Ajtai, K., Reisler, E., and Burghardt, T. P. (2003) *Biophys. J. 84*, 1047−1056.

BI026183E